OPEN ACCESS
IOP Publishing
Journal of Physics B: Atomic, Molecular and Optical Physics
J. Phys. B: At. Mol. Opt. Phys. **57** (2024) 235203 (13pp)
https://doi.org/10.1088/1361-6455/ad8aaf

Back-decay of the muonic molecular ion $(\alpha\mu t)^{2+}_{01}$ resonantly formed in $(t\mu)_{1s} + {}^4\mathrm{HeH}^+$ collision

Wilhelm Czapliński

Department of Applied Nuclear Physics, AGH University of Krakow, al. Mickiewicza 30, 30-059 Kraków, Poland

E-mail: gjczapli@cyf-kr.edu.pl

Received 19 March 2024, revised 16 August 2024
Accepted for publication 23 October 2024
Published 1 November 2024

Abstract

Resonant formation of the muonic molecular ion $(\alpha\mu t)^{2+}_{01}$ in the collision of the muonic tritium atom with the helium hydride ion, $(t\mu)_{1s} + {}^4\mathrm{HeH}^+ \rightarrow [(\alpha\mu t)^{2+}_{01}, p, ee]^+$, is proposed. The $(\alpha\mu t)^{2+}_{01}$ ion is formed in the rotational-vibrational state (0,1) as one of the two nuclei of the final complex. Back-decay process $[(\alpha\mu t)^{2+}_{01}, p, ee]^+_{Kn} \rightarrow (t\mu)_{1s} + {}^4\mathrm{HeH}^+_{K'n'}$, where K and n ($K'$and n') is the rotational and vibrational quantum number, respectively, is considered in detail and the corresponding decay widths for all possible rotational-vibrational $(K,n) \rightarrow (K',n')$ transitions are calculated. Numerous inelastic decay channels of $(\alpha\mu t)^{2+}_{01}$ are also presented and discussed. The possible fast resonant formation of the $(\alpha\mu t)^{2+}_{01}$ ion may provide an interesting tool for experimental studies of $t(\alpha,\gamma)^7\mathrm{Li}$ nuclear fusion, which is one of the most important reactions in Big-Bang nucleosynthesis models. Studying this reaction may prove important for solving the lithium problem.

Keywords: nuclear fusion, muonic molecules, hydrohelium, back-decay, Big-Bang nucleosynthesis, lithium problem

1. Introduction

Negative muon μ^- entering a gaseous mixture of light elements initiates several different atomic and molecular processes during its short lifetime $\tau_\mu = 2.197 \times 10^{-6}$ s [1]. The most basic processes include the formation of muonic atoms and muon transfer from lighter to heavier elements, formation of muonic molecular ions (usually called muonic molecules) and fusion of the muonic molecule nuclei [2–4]. These processes form an unavoidable background in experimental investigations of weak muon capture, which provides information on important issues such as the structure of light nuclei, exchange-current effects, T-violation [5–9], proton pseudoscalar coupling constant g_P [10], solar p-p fusion [11, 12], neutrino–hydrogen and neutrino–deuterium scattering [13]. Extensive experimental research has been carried out to solve the puzzle of the proton charge radius [14–16] by precisely measuring the Lamb-shift in the $p\mu$ atom [17] (henceforth, the negative muon is called a muon and denoted by μ). However, among the processes involving muons, the most spectacular seems to be the fusion of the nuclei of muonic molecules. The molecules composed of hydrogen or hydrogen and helium isotopes [18–23]: $(p\mu d)^+$, $(d\mu d)^+$, $(d\mu t)^+$, $({}^3\mathrm{He}\mu d)^{2+}$, $({}^4\mathrm{He}\mu t)^{2+}$, etc, are so small (the internuclear separation is about 0.03–0.07 in atomic units, au) that their nuclei can tunnel through the Coulomb barrier and fuse. Therefore,

muonic molecules provide the opportunity to study nuclear reactions at low energies, especially because the quantum states of these molecules can be controlled using superintense laser fields [24, 25]. At the same time, the main difficulty in laboratory studies of nuclear reactions of light elements in low-energy scattering experiments is related to the Coulomb repulsion, which causes high uncertainty in the measured reaction rates. These studies typically aim to calculate the corresponding reaction rates and astrophysical *S*-factors [26], which are used in Big Bang nucleosynthesis (BBN) models [27–35] to understand the abundance of light elements in the universe. In particular direct radiative capture $t(\alpha,\gamma)^7\mathrm{Li}$ at energies of interest in the range of 0–500 keV belongs to the set of the most important reactions [33–39]. It is known that the bulk of ^{7}Li is unrelated to galactic nucleosynthesis and is thus primordial [37]. According to the standard BBN model ^{7}Li is produced mainly in two-step process [31]: first ^{7}Be is produced in radiative capture $^3\mathrm{He}(\alpha,\gamma)^7\mathrm{Be}$ then, long after BBN ceases, due to electron capture $^7\mathrm{Be}\rightarrow{}^7\mathrm{Li}$. The second source of ^{7}Li is the radiative capture $t(\alpha,\gamma)^7\mathrm{Li}$. Consequently, the ^{7}Li abundance sums both mass-7 isotopes. Experimental and theoretical investigations of the $t(\alpha,\gamma)^7\mathrm{Li}$ reaction are important in the context of the lithium problem [30, 36, 37, 40]. Namely, the relative abundance $^7\mathrm{Li}/\mathrm{H}$ predicted by the standard BBN models, $(4.283+0.335-0.292)\times10^{-10}$, is approximately three times greater than that obtained from observations of metal-poor halo stars $(1.58+0.35-0.28)\times10^{-10}$ [36, 37] and references therein (predictions of the abundance of ^{6}Li are also controversial). To eliminate this discrepancy, a number of attempts have been made in astrophysical, nuclear, and beyond standard model measurements resorting to new particle and cosmological physics [30, 36, 37, 41–45]. Existing experimental results for the *S*-factor corresponding to the $t(\alpha,\gamma)^7\mathrm{Li}$ reaction are divergent at collision energies $50\,\mathrm{keV}<E<500\,\mathrm{keV}$ and do not cover energies below 50 keV (see [46–49] and references therein). Similarly, theoretical results show qualitative and quantitative discrepancies [47–56]. Therefore, experimental studies of the $t(\alpha,\gamma)^7\mathrm{Li}$ reaction are important for verifying theoretical models of low-energy ^{4}He - t nuclear interactions, as well as for determining whether a solution to the lithium problem should be sought outside the standard model.

Muonic molecules composed of isotopes of hydrogen and helium, $(\mathrm{He}\mu h)^{2+}$, where $\mathrm{He}={}^3\mathrm{He},{}^4\mathrm{He}$ and $h=p,\,d,\,t$, are Feshbach resonances in $(\mathrm{He}\mu)^+_{1s}+h$ collisions at energies of several keV [57–67]. The resonances are formed due to excitation of the three-body $\mathrm{He}^{2+}-\mu-h$ system from the ground $1s\sigma$ state, which corresponds asymptotically to the $(\mathrm{He}\mu)^+_{1s}+h$ system, to some excited states. Resonances below the $(h\mu)_{1s}$ thresholds correspond to excitation from the ground to the excited $2p\sigma$ state, which asymptotically corresponds to the $\mathrm{He}^{2+}+(h\mu)_{1s}$ system. These resonances are characterized by the rotational $j=0,1,2$ and vibrational $\nu=0,1$ quantum numbers, with the only resonance in the excited vibrational $\nu=1$ state being the $(\alpha\mu t)^{2+}_{j=0,\nu=1}$ resonance [62, 68], denoted by $(\alpha\mu t)^{2+}_{01}$ in the following. The resonances in the vibrational ground state, $(\mathrm{He}\mu h)^{2+}_{j,0}$ ($j=2$ is excluded for $h=p$), are well below the corresponding $(h\mu)_{1s}$ thresholds and can be formed in helium ionization process $(h\mu)_{1s}+\mathrm{He}\rightarrow[(\mathrm{He}\mu h)^{2+}_{j,0},e]^+ + e$ at any low collision energy [18, 68]. In contrast, the $(\alpha\mu t)^{2+}_{01}$ resonance is only 0.13 eV below the $(t\mu)_{1s}$ threshold[1] [62]. In principle, this molecule could be formed also in helium ionization process, but a high collision energy required, comparable to the helium ionization potential, 24.6 eV, makes this process very unlikely. Another formation of the $(\alpha\mu t)^{2+}_{01}$ is three-body collision [69] $(t\mu)_{1s}+{}^4\mathrm{He}+{}^4\mathrm{He}\rightarrow[(\alpha\mu t)^{2+}_{01},2e]+{}^4\mathrm{He}$. However, the corresponding effective formation rate is relatively low ($\sim10^7\,\mathrm{s}^{-1}$) even for high helium concentrations, which are comparable to the liquid hydrogen concentration, $\mathrm{LHD}=4.25\times10^{22}\,\mathrm{cm}^{-3}$. It is easy to see that the weakly bound $(\alpha\mu t)^{2+}_{01}$ reminds the weakly bound muonic molecules $(d\mu d)^+_{11}$ and $(d\mu t)^+_{11}$ in rotational and vibrational (rovibrational in the following) states $(j,\nu)=(1,1)$. These states were discovered in [22] using the adiabatic representation for the three-body Coulomb problem. Binding energies: 1.946 eV for $(d\mu d)^+_{11}$ and 0.634 eV for $(d\mu t)^+_{11}$, were calculated in [23]. These molecules can be formed in fast resonant processes in collisions of $(d\mu)_{1s}$ and $(t\mu)_{1s}$ atoms with electronic hydrogen molecules, e.g. $(t\mu)_{1s}+\mathrm{D}_2\rightarrow[(d\mu t)^+_{11},d,ee]_{Kn}$. The excess energy is transferred to rotational (K) and vibrational (n) degrees of freedom of the final complex, which resembles the ordinary D_2 molecule but with the $(d\mu t)^+_{11}$ as one of its two nuclei. The $(d\mu t)^+_{11}$ formation rate as a function of kinetic energy of $(t\mu)_{1s}$ atom reaches (after normalization to LHD) a very high value, which is of the order of $10^{10}\,\mathrm{s}^{-1}$ [70]. Similarly, the $(\alpha\mu t)^{2+}_{01}$ molecule is expected to be formed in fast resonant process in collision of the $(t\mu)_{1s}$ atom with some ^{4}He-containing molecular system. A good candidate for such a system is helium hydride ion, $^4\mathrm{HeH}^+$, which rovibrational excitation energies are comparable to the $(\alpha\mu t)^{2+}_{01}$ binding energy, 0.13 eV. The proposed resonant process

$$(t\mu)_{1s}+{}^4\mathrm{HeH}^+_{Kn}\rightarrow\left[(\alpha\mu t)^{2+}_{01},p,ee\right]^+_{K'n'} \tag{1}$$

leads to the formation of an excited final molecular complex $[(\alpha\mu t)^{2+}_{01},p,ee]^+_{K'n'}$ with $(\alpha\mu t)^{2+}_{01}$ as one of its two nuclei; (K,n) and (K',n') are rovibrational quantum numbers of $^4\mathrm{HeH}^+$ and the final complex, respectively. The following, the final complex is denoted as $\mathrm{M}_{01}\mathrm{H}^+$, where M^{2+}_{01} is $(\alpha\mu t)^{2+}_{01}$.

It is interesting to note that the $^4\mathrm{HeH}^+$ ion, one of the most elementary molecular systems [71], was first observed in 1925 in the mass spectrum of discharges in a mixture of helium and hydrogen [72]. The ion was identified by its charge-to-mass ratio $q/m=(1/5)(e/m_p)$, where m_p is the proton mass. The ion can be relatively easily synthesized and handled in He–H

[1] This value includes relativistic correction (+4 meV) resulting from the vacuum polarization [62].

mixtures using various experimental techniques, such as discharge through the mixture [73], electron-impact ionization [74] with an electrostatic ion trap [75, 76], hollow-cathode ion source [77, 78], electrostatic low-energy storage ring [79], and duoplasmotron ion source [80, 81].

The HeH^+ ion appears in models of the early universe as the first molecular system primarily formed due to radiative association $He + H^+ \rightarrow HeH^+ + \gamma$ [82–86]. The ion is also expected to be formed in planetary nebulae by the radiative association of He^+ with H in the transition region of space between the fully ionized and neutral zones [87, 88]. Because hydrogen and helium are two of the most abundant elements in the Universe, the ion was considered potentially detectable [89–91]. However, because of the insufficient resolution of spectrometers, HeH^+ radiation lines have not been observed in astronomical spectra over the last few decades [92–94]. The ion was recently detected in the planetary nebula NGC 7027 by observing the fundamental rotational $J = 1$–0 line in the Stratospheric Observatory for Infrared Astronomy [95], as well as by observing the rovibrational $\nu = 1-0\, P(1)$ and $P(2)$ lines with the iSHELL spectrograph at NASA's Infrared telescope facility on Maunakea [96].

To calculate the cross-section for resonant formation (1), the widths of the $(\alpha\mu t)^{2+}_{01}$ decay channels must first be calculated (see [97–100], where calculations of cross-sections for resonant $(d\mu d)^+_{11}$ and $(d\mu t)^+_{11}$ formation are presented). The crucial decay channel is back-decay

$$M_{01}H^+_{Kn} \rightarrow (t\mu)_{1s} + {}^4HeH^+_{K'n'}, \qquad (2)$$

that which restores the muonic tritium atom in the ground state and the $^4HeH^+$ ion in an excited rovibrational (K', n') state.

This paper is arranged as follows: the method of calculating the back-decay width is presented in section 2; the results obtained are presented and discussed in section 3, where other $(\alpha\mu t)^{2+}_{01}$ decay channels are also discussed. Unless otherwise noted, au are used in the text.

2. Method of calculation

2.1. The $(\alpha\mu t)^{2+}_{01}$ muonic molecule

The energy levels of the $(He\mu h)^{2+}_{j,0}$ muonic molecules lie relatively deep below the corresponding $(h\mu)_{1s}$ thresholds and can be described using adiabatic approximation as bound states in the $2p\sigma$ potential [18,19, 101]. The corresponding wave functions, which are eigenfunctions of the square of the total angular momentum $\hat{\mathbf{j}}$ and its z-axis projection $\hat{j}_z$, have the form

$$\phi^{\rm mol}_{jm_j\nu}(\mathbf{R},\mathbf{r}) = \varphi^{\mu}_{2p\sigma}(R;\mathbf{r})\,\chi_{j\nu}(R)\,R^{-1}Y_{jm_j}\left(\hat{\mathbf{R}}\right), \qquad (3)$$

where j and m_j are the respective quantum numbers; ν is vibrational quantum number; vectors $\mathbf{R}$ and $\mathbf{r}$ are defined in figure 1(a); $\varphi^{\mu}_{2p\sigma}(R;\mathbf{r})$ is the two center wave function of the muon in the Coulomb fields of the two fixed nuclei He^{2+} and h, separated by R; $\chi_{j\nu}(R)$ is the radial function describing the relative $He^{2+} - h$ motion; $Y_{jm_j}(\hat{\mathbf{R}})$ is spherical harmonic [102]; $\hat{\mathbf{R}} = \mathbf{R}/R$.

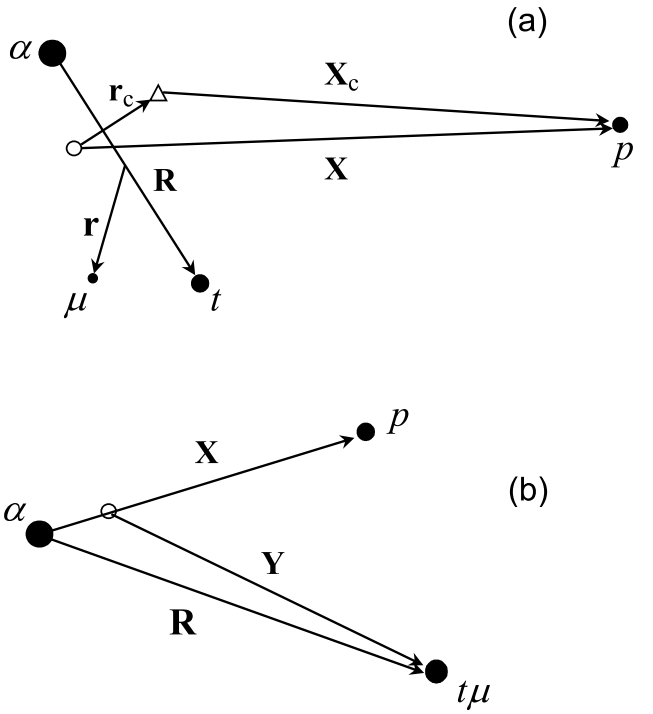

Figure 1. Coordinates used in description of the initial (a) and the final (b) state of the back decay (2). (a) Vector $\mathbf{r}$ connects the middle of $\mathbf{R}$ with the muon. Triangle denotes the center of charge of the $(\alpha\mu t)^{2+}_{01}$. Open circle denotes the center of mass of the muonic molecule (a) and the $^4HeH^+$ ion (b).

The muonic wave function $\varphi^{\mu}_{2p\sigma}(R;\mathbf{r})$ tends in the $R \rightarrow 0$ limit (the united-atom limit) to the wave function of the $(Li\mu)^{2+}$ ion in the excited $(n,l,m) = (2,1,0)$ state, whereas in the $R \rightarrow \infty$ limit (the separated-atoms limit) $\varphi^{\mu}_{2p\sigma}(R;\mathbf{r})$ tends to the $(h\mu)_{1s}$ atomic wave function [103]. Since the $(\alpha\mu t)^{2+}_{01}$ molecule is weakly bound, the corresponding radial function $\chi_{01}(R)$ extends over long distances and is therefore very sensitive to the details of the potential. Adiabatic approximation is insufficient in this case [69], and more sophisticated calculations are required. This calculation was performed in [62] using the coupled rearrangement channel method [104], which exploits the variational function spanned over wave functions corresponding to $(\alpha\mu) + t$, $(\alpha t) + \mu$, and $\alpha + (t\mu)$ channels. The results show that muon in the $(\alpha\mu t)^{2+}_{01}$ molecule is strongly clustered on triton with less than 0.4% of its energy being due to the admixture of $\alpha\mu$ orbital. Thus, the muonic molecule strongly resembles the $\alpha + (t\mu)_{1s}$ system. Since the $\varphi^{\mu}_{2p\sigma}(R;\mathbf{r})$ for large R is the $(t\mu)_{1s}$ wave function, the $(\alpha\mu t)^{2+}_{01}$ wave function can be approximated by (3) for $(j,\nu) = (0,1)$ and $\chi_{01}(R)$ taken from [62]. The average $\alpha - t$ separation, $\bar{R} = \int_0^\infty (\chi_{01}(R))^2 dR$, is equal to 0.07 au, making this molecule approximately four to five times larger than $(He\mu h)^{2+}_{j0}$ molecules.

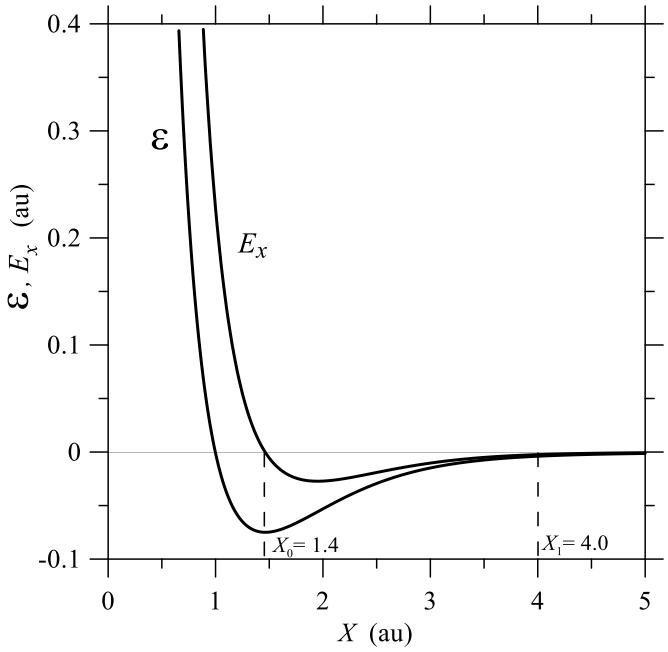

Figure 2. Born–Oppenheimer potential $\mathsf{E}(X)$ for the ground electronic $^1\Sigma^+$ state of the $^4HeH^+$ ion [106] and the corresponding electric field $E_x(X) = -Z_{\rm mol}^{-1} d\mathsf{E}(X)/dX$.

2.2. The $^4HeH^+$ and $M_{01}H^+$ ions

The ions were described by the Born–Oppenheimer (B–O) approximation. The wave function of the $^4HeH^+$ in the ground electronic $^1\Sigma^+$ state was chosen as an eigenfunction of the square of the total angular momentum operator $\hat{\mathbf{K}}$ and its z-axis projection $\hat{K}_z$ [105]

$$\Psi^{\rm ion}_{KM_K n}(\mathbf{X},\mathbf{r}_1,\mathbf{r}_2) = \varphi_{\rm e}(X,\mathbf{r}_1,\mathbf{r}_2)\ \Phi^{\rm rel}_{KM_K n}(\mathbf{X}), \qquad (4)$$

where K and M_K are the corresponding quantum numbers, n is vibrational quantum number, vector $\mathbf{X}$ connects the α particle with the proton, $\mathbf{r}_1$ and $\mathbf{r}_2$ are the position vectors of two electrons, and $\varphi_{\rm e}(X,\mathbf{r}_1,\mathbf{r}_2)$ is the electronic $^1\Sigma^+$ state wave function. Function $\Phi^{\rm rel}_{KM_K n}(\mathbf{X})$ describes relative $\alpha - p$ motion,

$$\Phi^{\rm rel}_{KM_K n}(\mathbf{X}) = X^{-1}\xi_{Kn}(X)\, Y_{KM_K}\left(\hat{\mathbf{X}}\right), \qquad (5)$$

where $\xi_{Kn}(X)$ is a bound state solution of the radial Schrödinger equation with the potential [106] corresponding to the $^1\Sigma^+$ molecular term. The potential is denoted here as $\mathsf{E}(X)$ and is presented in figure 2. The average $\alpha - p$ separation in the ground rovibrational state, $\bar{X} = \int_0^\infty {\rm d}X X \xi^2_{00}(X)$, equals 1.52 au.

The coordinates used to describe the $M_{01}H^+$ ion are shown in figure 1(a). Because the ratio of the average internuclear separations in $(\alpha\mu t)^{2+}_{01}$ and $^4HeH^+$ is $\bar{R}/\bar{X} \approx 0.05 << 1$, the muonic molecule is considered a heavy nucleus of the $M_{01}H^+$ ion. The electric charge distribution in the muonic molecule $(\alpha\mu t)^{2+}_{01}$ is not spherically symmetric; however, the potential generated by the molecule at distances $X_{\rm c} \sim \bar{X}$ from its center of charge is close to the Coulomb potential $2/X_{\rm c}$. This is because the dipole term of the multipole expansion of the potential vanishes identically, whereas the higher order terms (quadrupole, octupole, etc) are small and can be neglected because of the small value of the $\bar{R}/\bar{X}$ ratio. Consequently, the two electrons of the $M_{01}H^+$ ion move in the electric field of two point-like charges, that is the charge of the muonic molecule $Z_{\rm mol} = 2$ and the charge of the proton, separated by $X_{\rm c}$. The energy of the electrons $\mathcal{E}(X_{\rm c})$ (molecular term) is a function of $X_{\rm c}$. On the other hand, the rovibrational degrees of freedom of $M_{01}H^+$ are related to vector $\mathbf{X} = \mathbf{r}_{\rm c} + \mathbf{X}_{\rm c}$, which connects the center of mass of the muonic molecule with the proton, $\mathbf{r}_{\rm c}$ connects the center of mass of $(\alpha\mu t)^{2+}_{01}$ with its center of charge. Expanding $\mathcal{E}(X_{\rm c})$ in the power series of $r_{\rm c}/X$ to the dipole term, we obtain $\mathcal{E}(X_{\rm c}) = \mathsf{E}(X) + V_{\rm bd}$, where

$$V_{\rm bd} = -\,\mathbf{d}\cdot\mathbf{E}(\mathbf{X}) \qquad (6)$$

and

$$\mathbf{E}(\mathbf{X}) = -\hat{\mathbf{X}} Z^{-1}_{\rm mol} d\mathsf{E}(X)/dX \qquad (7)$$

is the electric field of the two electrons and the proton in the $(\alpha\mu t)^{2+}_{01}$ center of mass [107]; $\mathbf{d} = Z_{\rm mol}\mathbf{r}_{\rm c}$ is the dipole moment of the muonic molecule relative to it center of mass. It is convenient to express the dipole moment by vectors $\mathbf{r}$ and $\mathbf{R}$, $\mathbf{d} = -\,(a_1\mathbf{R} + a_2\mathbf{r})$, where $a_1 = 1/2 - (m_\alpha - m_t)/m_{\rm mol}$, $a_2 = 1 + 2m_\mu/m_{\rm mol}$, $m_{\rm mol} = m_\alpha + m_t + m_\mu$, and m_α, m_t, m_μ are masses of the muonic molecule components. The x-coordinate of the electric field, $E_x(X) = \hat{\mathbf{X}}\cdot\mathbf{E}(\mathbf{X})$, is shown in figure 2. For further calculations, it is convenient to assume that the muonic molecule is in a rovibrational (j,ν) state, $(\alpha\mu t)^{2+}_{j\nu}$. The ion, that includes the muonic molecule is denoted by $M_{j\nu}H^+_{Kn}$, where $M^{2+}_{j\nu}$ stands for $(\alpha\mu t)^{2+}_{j\nu}$. If the size of the muonic molecule is neglected then $\mathbf{X} = \mathbf{X}_{\rm c}$ and, consequently, the total angular momentum operator of $M_{j\nu}H^+_{Kn}$ can be expressed as

$$\hat{\mathbf{j}} = \hat{\mathbf{j}} + \hat{\mathbf{K}}, \qquad (8)$$

where $\hat{\mathbf{j}}$ and $\hat{\mathbf{K}}$ are the total angular momentum operator of the muonic molecule and the $M_{j\nu}H^+_{Kn}$ ion (with $(\alpha\mu t)^{2+}_{j\nu}$ as a point-like nucleus), respectively. Moreover, in this approximation, the electronic wave-functions and molecular terms of the $^4HeH^+$ and $M_{j\nu}H^+$ ions are identical. The wave function of $M_{j\nu}H^+_{Kn}$, which is an eigenfunction of $\hat{\mathbf{j}}^2$ and $\hat{J}_z$, has the form

$$\begin{aligned}\Psi^{\rm ion}_{j\nu KnJM_J} &= \left\{\phi^{\rm mol}_{j\nu}(\mathbf{R},\mathbf{r}) \otimes \Psi^{\rm ion}_{Kn}(\mathbf{X},\mathbf{r}_1,\mathbf{r}_2)\right\}_{JM_J} \\ &= \varphi_{\rm e}(X,\mathbf{r}_1,\mathbf{r}_2)\sum_{m_j M_K} C^{JM_J}_{jm_jKM_K}\phi^{\rm mol}_{jm_j\nu}(\mathbf{R},\mathbf{r})\,\Phi^{\rm rel}_{KM_K n}(\mathbf{X}),\end{aligned} \qquad (9)$$

where $\phi^{\rm mol}_{jm_j\nu}(\mathbf{R},\mathbf{r})$, $\Psi^{\rm ion}_{KM_K n}(\mathbf{X},\mathbf{r}_1,\mathbf{r}_2)$, and $\Phi^{\rm rel}_{KM_K n}(\mathbf{X})$ are defined in (3), (4), and (5), respectively; quantum numbers (J,M_J) and (K,M_K) correspond to $(\hat{\mathbf{j}}^2,\hat{J}_z)$ and $(\hat{\mathbf{K}}^2,\hat{K}_z)$, respectively; and $C^{JM_J}_{jm_jKM_K}$ are Clebsch–Gordan coefficients [108].

2.3. Back-decay

The transition matrix element calculated in the first order of perturbation theory with potential (6), which is responsible for the back-decay process, $T_{\rm fi} = \langle \Psi_{\rm f} | V_{\rm bd} | \Psi_{\rm i} \rangle$, involves wave functions of the entire system in the initial (i) and final (f) states, calculated in the zero-order approximation. This means that $\Psi_{\rm i}$ is expressed by (9), and $\Psi_{\rm f}$ must be calculated by neglecting the dimension of the $(t\mu)_{1s}$ atom, $r_{t\mu}$, because it fulfills the condition $r_{t\mu} << r_{\rm c} << X$. $\Psi_{\rm i}$ and $\Psi_{\rm f}$ are chosen as eigenfunctions of the square of the total angular momentum operator of the entire system $\hat{\mathbf{j}}$ and its z-axis projection $\hat{J}_z$. In the initial state of process (2), the total angular momentum operator $\hat{\mathbf{j}}$ is defined as in (8). In the final state of (2), $\hat{\mathbf{j}}$ is the sum $\hat{\mathbf{J}} = \hat{\mathbf{K}} + \hat{\mathbf{L}}$, where $\hat{\mathbf{K}}$ is the angular momentum of the nuclei of the ^{4}HeH$^+$ ion and $\hat{\mathbf{L}}$ is the angular momentum of the relative ^{4}HeH$^+ - (t\mu)_{1s}$ motion. The quantum numbers corresponding to $(\hat{\mathbf{j}}^2, \hat{J}_z)$, $(\hat{\mathbf{K}}^2, \hat{K}_z)$, and $(\hat{\mathbf{L}}^2, \hat{L}_z)$ are (J, M_J), (K', M'_K) and (L', M'_L), respectively. The final state wave function has the form

$$\begin{aligned}\Psi_{\rm f} &= u_{1s}^{t\mu}(\mathbf{r}_\mu)\left\{\Omega_{pL'}(\mathbf{Y}) \otimes \Phi^{\rm rel}_{K'n'}(\mathbf{X})\right\}_{JM_J} \\ &= u_{1s}^{t\mu}(\mathbf{r}_\mu) \sum_{M'_L M'_K} C^{JM_J}_{L'M'_L K'M'_K} \Omega_{pL'M'_L}(\mathbf{Y})\, \Phi^{\rm rel}_{K'M'_K n'}(\mathbf{X}),\end{aligned} \tag{10}$$

where $\Phi^{\rm rel}_{K'M'_K n'}(\mathbf{X})$ is defined in (5); $u_{1s}^{t\mu}(\mathbf{r}_\mu)$ is the ground state orbital of the $(t\mu)_{1s}$ atom; $\Omega_{pL'M'_L}(\mathbf{Y})$ is the spherical wave describing the relative ^{4}HeH$^+ - (t\mu)_{1s}$ motion with momentum p in the rotational (L', M'_L) state; $\mathbf{Y}$ is defined in figure 1(b) as the vector connecting the center of mass of ^{4}HeH$^+$ with $(t\mu)_{1s}$. Function $\Omega_{pL'M'_L}(\mathbf{Y})$ is calculated by neglecting the interaction between the two systems because $(t\mu)_{1s}$ is small and neutral

$$\Omega_{pL'M'_L}(\mathbf{Y}) = 2pj_{L'}(pY)\, Y_{L'M'_L}\left(\hat{\mathbf{Y}}\right), \tag{11}$$

where $j_{L'}(x)$ is a spherical Bessel function [109]. The following normalization condition is fulfilled $\langle \Omega_{p_1 L'_1 M'_{L_1}} | \Omega_{p_2 L'_2 M'_{L_2}} \rangle = 2\pi\,\delta(p_1 - p_2)\delta_{L'_1 L'_2}\delta_{M'_{L_1} M'_{L_2}}$. In can be inferred from figure 1(b) that $\mathbf{Y} = \mathbf{R} - b\mathbf{X}$, where $b = m_p/(m_p + m_\alpha)$, and m_p is the proton mass. It is useful to expand function (11) into the series of bipolar spherical harmonics [110]

$$\begin{aligned}&\Omega_{pL'M'_L}(\mathbf{Y}) \\ &= 2\sqrt{4\pi}\, p \sum_{l_1, l_2} (-1)^{l_1} \sqrt{(2l_1+1)(2l_2+1)} \begin{pmatrix} l_1 & l_2 & L' \\ 0 & 0 & 0 \end{pmatrix} \cdot \\ &\quad \times j_{l_1}(pR) j_{l_2}(bpX) \left\{ Y_{l_1}\left(\hat{\mathbf{R}}\right) \otimes Y_{l_2}\left(\hat{\mathbf{X}}\right) \right\}_{L'M'_L}\end{aligned} \tag{12}$$

This allows the calculation of the transition matrix element without the approximations used in [70]. The transition matrix element $T_{\rm fi}$, calculated using wave functions (9) and (10) receives the form

$$T_{\rm fi} = -\langle pK'n'L'; JM_J | \mathbf{d}^{\rm av} \cdot \mathbf{E} | \nu j K n; JM_J \rangle, \tag{13}$$

where $\mathbf{d}^{\rm av} = \langle u_{1s}^{t\mu} | \mathbf{d} | \varphi^{\mu}_{2p\sigma} \rangle_\mu$, the subscript μ denoted integration over the muon coordinates only. Because $\varphi^{\mu}_{2p\sigma}(R; \mathbf{r})$ tends for a large R to the wave function of the $(t\mu)_{1s}$ atom, $\mathbf{d}^{\rm av}$ is taken in the form

$$\mathbf{d}^{\rm av} = \left\langle \varphi^{\mu}_{2p\sigma} \middle| \mathbf{d} \middle| \varphi^{\mu}_{2p\sigma} \right\rangle_\mu = -D(R)\,\hat{\mathbf{R}}, \tag{14}$$

where $D(R) = a_R R + a_r \langle \varphi^{\mu}_{2p\sigma} | \mathbf{r} \cdot \hat{\mathbf{R}} | \varphi^{\mu}_{2p\sigma} \rangle_\mu$. After substituting (12) and (14) into (13), and taking into account that $(j, \nu) = (0, 1)$, $T_{\rm fi}$ takes its final form

$$\begin{aligned}T_{\rm fi} &= 2\, i^{K'+K-L'} \sqrt{(2L'+1)(2K'+1)} \\ &\quad \times \begin{pmatrix} L' & K' & K \\ 0 & 0 & 0 \end{pmatrix} p I_{\rm mol}(p)\, I^{\rm ion}_{L'K'n'Kn}(bp),\end{aligned} \tag{15}$$

where

$$I_{\rm mol}(p) = \int_0^\infty {\rm d}R j_1(pR)\, RD(R)\, \chi_{01}(R); \tag{16}$$

$$I^{\rm ion}_{L'K'n'Kn}(bp) = \int_0^\infty {\rm d}X \xi_{K'n'}(X) \left({\rm d}j_{L'}(z)/{\rm d}z\right) E_x(X)\, \xi_{Kn}(X); \tag{17}$$

and $z = bpX$.

The formula for the back-decay [111] is

$$\Gamma = 2\pi \sum_{L'} \int \frac{{\rm d}p}{2\pi} |T_{\rm fi}|^2 \delta(E_{\rm f} - E_{\rm i}), \tag{18}$$

where $E_{\rm i} = E_{Kn} + \epsilon_{01}$ and $E_{\rm f} = E_{K'n'} + p^2/(2m_{\rm r})$ are the energies of the entire system in the initial and final states, respectively; E_{Kn} and $E_{K'n'}$ are the rovibrational energies of $M_{01}H^+_{Kn}$ and ^{4}HeH$^+_{K'n'}$, respectively; $\epsilon_{01} = -0.13$ eV is the energy of the $(\alpha\mu t)^{2+}_{01}$ molecule relative to the $(t\mu)_{1s}$ threshold; and $m_{\rm r}$ is the reduced mass of the ^{4}HeH$^+ + (t\mu)_{1s}$ system. After substituting (15) into (18), the back-decay width takes the final form

$$\Gamma^{\rm bd}_{K'n'Kn} = 4 m_{\rm red} p_{\rm r} I^2_{\rm mol}(p_{\rm r}) \sum_{L'=|K-K'|}^{K+K'} G_{L'K'K} \left(I^{\rm ion}_{L'K'n'Kn} \right)^2, \tag{19}$$

where

$$G_{L'K'K} = (2L'+1)(2K'+1) \begin{pmatrix} L' & K' & K \\ 0 & 0 & 0 \end{pmatrix}^2 \tag{20}$$

is geometrical factor; $I^{\rm ion}_{L'K'n'Kn} \equiv I^{\rm ion}_{L'K'n'Kn}(bp_{\rm r})$, and $p_{\rm r} = \sqrt{2m_{\rm r}(\epsilon_{01} + E_{Kn} - E_{K'n'})}$ is the resonant momentum.

Table 1. The ten fastest back-decay transitions, the corresponding resonant energies ε_r, and widths. $\Gamma^{bd}_{K'n'Kn}$ was calculated according to (19), whereas approximated width $\gamma^{bd}_{K'n'Kn}$ was calculated according to (21) (see this Section below).

$(K,n)\to(K',n')$		ε_r(eV)	$\Gamma^{bd}_{K'n'Kn}$(meV)	$\gamma^{bd}_{K'n'Kn}$(meV)
(1,3)	(1,2)	0.111	2.95	2.42
(1,2)	(1,1)	0.157	2.81	2.36
(2,3)	(2,2)	0.109	2,75	2.36
(2,2)	(2,1)	0.155	2.66	2.32
(3,3)	(3,2)	0.105	2.63	2.28
(3,2)	(3,1)	0.151	2.57	2.27
(4,3)	(4,2)	0.101	2.50	2.17
(4,2)	(4,1)	0.146	2.49	2.20
(0,3)	(0,2)	0.112	2.45	2.45
(5,2)	(5,1)	0.140	2.39	2.11

3. Results and discussion

The energies and radial functions of the bound states of the $^4HeH^+$ and $M_{01}H^+$ ions were calculated by solving the Schrödinger equation with the B-O potential, $\mathsf{E}(X)$, that is presented in [106] (rovibrational resonant states [112, 113] were ignored in the present calculation). A common set of 160 pairs of rovibrational quantum states (K,n) was found for both the ions. The energies obtained for $^4HeH^+$ are very close to those presented in [114][2]. The energy levels of $M_{01}H^+$ lie slightly below those of $^4HeH^+$ because the ratio of the reduced mass of the nuclei of the first to the second ion is approximately 1.1. Because the centrifugal potentials of both ions are of the order of m_p^{-1} relative to the $\mathsf{E}(X)$ potential, the energies and radial functions depend very weakly on the rotational quantum numbers K and K'.

The resonance condition $\varepsilon_r = \in_{01} + E_{Kn} - E_{K'n'} > 0$ is fulfilled by 9631 rovibrational $(K,n)\to(K',n')$ transitions. Table 1 lists the ten largest widths in descending order. As can be seen, the widths correspond to $(K,n)\to(K,n-1)$ transitions, where K and n take small values. A maximum width 2.95 meV (reaction rate $\lambda = \Gamma/\hbar = 4.48\cdot 10^{12}\,s^{-1}$) corresponds to the $(1,3)\to(1,2)$ transition.

The back-decay width (19) depends on the rovibrational quantum numbers in a complicated manner. To analyze the corresponding results, it is convenient to use the quantum numbers K, n, and the differences $\Delta K = K - K'$ and $\Delta n = n - n'$. The results are presented in figure 3 in $(\Delta K,\Delta n)$ coordinates.

The widths are grouped into columns, the widths within a given column correspond to different pairs (K,n). The tallest columns, and therefore the largest widths, are located inside a rectangle, which can be conventionally defined by $|\Delta K|\leqslant 3$ and $1\leqslant\Delta n\leqslant 4$. All the widths outside this rectangle will be considered relatively small and will not be analyzed further. It is convenient to use the height of the $(\Delta K,\Delta n)$ column, that is the maximum width in the column, $\Gamma^{bd}_{max}(\Delta K,\Delta n) = \max_{K,n}\Gamma^{bd}_{K-\Delta K,n-\Delta n,Kn}$. The function $\Gamma^{bd}_{max}(\Delta K,\Delta n)$ has a maximum at $(\Delta K,\Delta n)=(0,1)$ and tends to decrease as Δn or $|\Delta K|$ increases. For a fixed $\Delta n\geqslant 1$, $\Gamma^{bd}_{max}(\Delta K,\Delta n)$ reaches its maximum at $\Delta K = 0$. It should be noted that transitions with $\Delta K\leqslant 2$ are allowed by resonance condition for $\Delta n\geqslant 1$, as seen in figure 3. Closer analysis of the results shows that the width within a given $(\Delta K,\Delta n)$ column, $\Gamma^{bd}_{K-\Delta K,n-\Delta n,Kn}$, considered as a function of K and n, has a maximum for some small K_0 and n_0, and is close to zero for large K or n. An example is given in figure 4, where the widths $\Gamma^{bd}_{K,n-1,Kn}$ corresponding to $(\Delta K,\Delta n)=(0,1)$ (see figure 3) are presented in (K,n) coordinates.

The main features of the results presented in figures 3 and 4 can be qualitatively explained by analyzing the integral $I^{ion}_{L'K'n'Kn}$ defined in (17). It can be assumed that the upper limit of the integral is finite because the electric field $E_x(X)$, and therefore the entire subintegral function, takes negligibly small values for a sufficiently large X (see figure 2). The integration interval can be chosen as $[0,X_1]$, where $X_1 = 4$. Moreover, the integral contains the function $dj_{L'}(z)/dz$ oscillating around zero [109], values of which decrease in the integration interval $[0,X_1]$ as L' increases. As a result, the square of the integral, $(I^{ion}_{L'K'n'Kn})^2$, tends to decrease as L' increases and, in most cases, the decrease is so fast that the sum in (19) is dominated by its first term for $L' = |\Delta K|$ (geometrical factor $G_{L'K'K}$ weakly depends on L'). Therefore, equation (19) can be simplified by leaving only the leading term

$$\gamma^{bd}_{K'n'Kn} = 4m_{red}\,Q_{K'n'Kn}\left(I^{ion}_{|\Delta K|K'n'Kn}\right)^2, \qquad (21)$$

where $Q_{K'n'Kn} = p_r I^2_{mol}(p_r) G_{|\Delta K|K'K}$. The corresponding results are presented in figure 5.

The comparison of figures 3 and 5 shows that the function $\Gamma^{bd}_{max}(\Delta K,\Delta n)$ is practically determined, as was to be expected, by the function $\gamma^{bd}_{max}(\Delta K,\Delta n)$, defined in analogous way. Formula (21) produces widths of which 86% have an accuracy greater than 80%, therefore, further analysis concerns $\gamma^{bd}_{K'n'Kn}$. Sample results are presented in the last column of table 1. It can be observed that the order of widths within the same columns in figures 3 and 5 (and also in table 1) are not identical.

The coefficients $(I^{ion}_{\Delta KK'n'Kn})^2$ and $Q_{K'n'Kn}$ in (21) are presented in figure 6 in the $(\Delta K,\Delta n)$ coordinates.

The heights of the corresponding columns are denoted as $I^2{}_{max}(\Delta K,\Delta n)$ and $Q_{max}(\Delta K,\Delta n)$. From the comparison of figures 5 and 6, it can be concluded that the shape of the $\gamma^{bd}_{max}(\Delta K,\Delta n)$ function is very similar to that of the $I^2{}_{max}(\Delta K,\Delta n)$ function, despite the presence of the $Q_{K'n'Kn}$ coefficients in (21). This can be qualitatively explained by the observation that $I^2{}_{max}(\Delta K,\Delta n)$ takes significant values and changes quickly in the area where $Q_{max}(\Delta K,\Delta n)$ changes relatively slowly $(\Delta K\geqslant 0)$, that is, in this area, the $Q_{K'n'Kn}$ coefficients belonging to different columns fall within similar ranges. Simultaneously, in the area where $Q_{max}(\Delta K,\Delta n)$ takes significant values and changes quickly $(\Delta K\leqslant -1)$, $I^2{}_{max}(\Delta K,\Delta n)$ is close to zero. This results in small values of

[2] $E_{20,0}$ and $E_{20,1}$ are missing in [114].

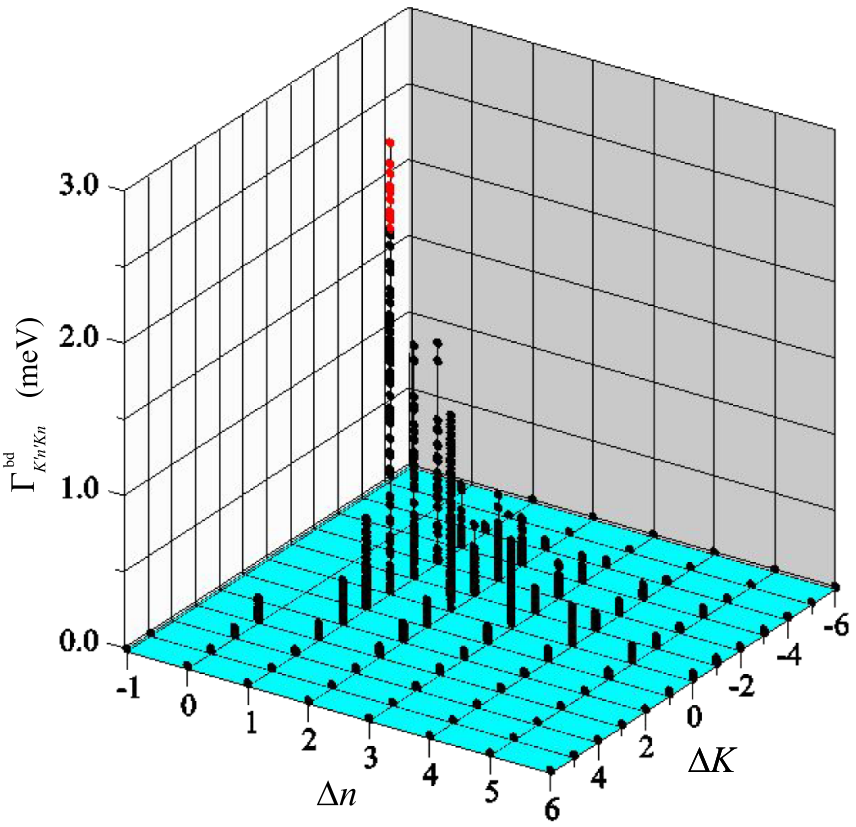

Figure 3. Back-decay widths on the $(\Delta K, \Delta n)$-plane (vertical lines help to read the coordinates). Red points represent the widths collected in table 1. Widths outside the range of both axes are close to zero.

$\gamma^{\rm bd}_{\rm max}(\Delta K, \Delta n)$ and, consequently, small values of $\gamma^{\rm bd}_{K'n'Kn}$ and $\Gamma^{\rm bd}_{K'n'Kn}$.

The integral $I^{\rm ion}_{L'K'n'Kn}$ depends on L' much more strongly than on other quantum numbers. The very weak dependence of $I^{\rm ion}_{L'K'n'Kn}$ on K and K' is due to the very weak dependence of the radial functions $\xi_{Kn}(X)$ and $\xi_{K'n'}(X)$ on K and K', respectively. Simultaneously, the relatively weak dependence of $I^{\rm ion}_{L'K'n'Kn}$ on n and n' can be explained by the observation that a significant contribution to the integral comes from the subinterval $[0, X_0]$, where $X_0 = 1.4$, in which the electric field $E_x(X)$ takes significant values (see figure 2). For example, if n increases and n' is fixed, there are two inherent and competing effects that change $(I^{\rm ion}_{L'K'n'Kn})^2$ in opposite directions: (a) radial function $\xi_{Kn}(X)$ occupies an increasingly larger area inside the potential well and penetrates deeper into the subinterval $[0, X_0]$. However, this effect saturates at a relatively small n. (b) The amplitude of $\xi_{Kn}(X)$ decreases in the entire integration interval $[0, X_1]$ because of the normalization of the radial function to unity. As a result of (a) and (b), $(I^{\rm ion}_{L'K'n'Kn})^2$ reaches its maximum value for some n_0 and tends to decrease as n increases. This is also true when n' increases and n is fixed, or when n and n' increase simultaneously in a given $(\Delta K, \Delta n)$ column.

Considering the above, it is understandable that the decrease in $I^2{}_{\rm max}(\Delta K, \Delta n)$ as $|\Delta K|$ increases for a fixed $\Delta n \geqslant 1$ is caused by the rapid decrease in $(I^{\rm ion}_{|\Delta K|K'n'Kn})^2$ as $|\Delta K|$ increases and the relatively weak dependence of $(I^{\rm ion}_{|\Delta K|K'n'Kn})^2$ on the remaining quantum numbers (in particular K and K'). As a result, $I^2{}_{\rm max}(\Delta K, \Delta n)$ has a maximum at $\Delta K = 0$. Note that transitions for $\Delta n \leqslant 0$ are allowed for $\Delta K \geqslant 3$ therefore, $I^2{}_{\rm max}(\Delta K, \Delta n)$ is small in this region.

At the same time, the Δn-dependence of $I^2{}_{\rm max}(\Delta K, \Delta n)$ for a fixed ΔK can be qualitatively explained by the observation that $n_{\rm top}$, which corresponds to $I^2{}_{\rm max}(\Delta K, \Delta n)$ in figure 6, tends to increase with increasing Δn and fixed ΔK, while $n'_{\rm top} = n_{\rm top} - \Delta n$ either tends to increase or remains constant. This is shown in table 2. Consequently, the $I^2{}_{\rm max}(\Delta K, \Delta n)$ for a fixed ΔK tends to decrease as Δn increases.

In addition to the back-decay (2) and decay of the muon, the $(\alpha\mu t)^{2+}_{01}$ molecule resonantly formed in process (1) can decay because of the $t(\alpha,\gamma)^7$Li fusion producing the exotic molecular system $[(^7{\rm Li}\mu)^{2+} pee]^+$. Another decay of $(\alpha\mu t)^{2+}_{01}$ is its deexcitation to the lower rovibrational (1,0) state or dissociation $(\alpha\mu t)^{2+}_{01} \rightarrow (\alpha\mu)^+_{1s} + t$ corresponding to the $2p\sigma \rightarrow 1s\sigma$ transition. These two processes can be accompanied by photon emission or ionization of the $M_{01}H^+$ ion however, nonradiative dissociation (predissociation) is also possible. This is summarized in figure 7. The energy released in the deexcitation and decay is 63.82 eV [62] and 5–8 keV [115, 116], respectively.

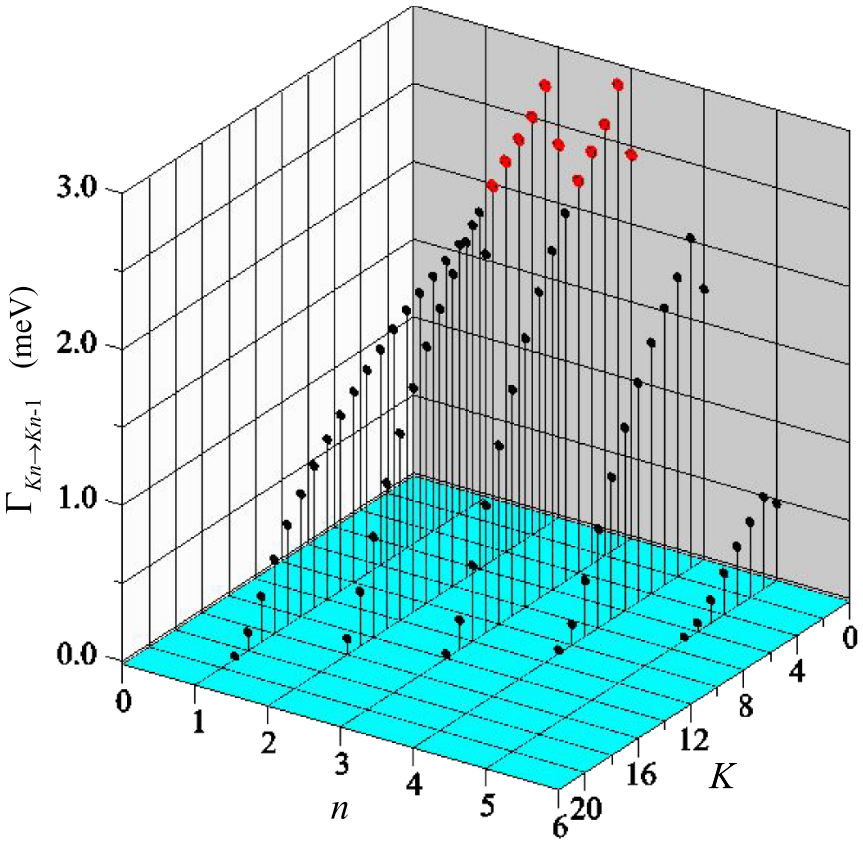

Figure 4. Back-decay widths corresponding to the $(\Delta K, \Delta n) = (0, 1)$ column (see figure 3) presented on (K,n)-plane. Red points represent the widths collected in table 1.

The photon-induced deexcitation, decay, and fusion, as well as predissociation can be described with a good approximation as occurring independently of the other components of the $M_{01}H^+$ ion, that is the proton and two electrons are spectators only. This is due to the small size of the muonic molecule compared to that of the electronic $M_{01}H^+$ ion. The width of the photon-induced deexcitation can be easily calculated using the standard approach for the E1 transition [117]. The result obtained, 8.34×10^{-10} eV ($\lambda = 1.27 \times 10^6\,\mathrm{s}^{-1}$), is on the order of the muon decay width, $\hbar\tau_\mu^{-1} \approx 3.0 \times 10^{-10}$ eV. The widths for photon-induced decay and predissociation can be calculated using the methods presented in [116, 118].

The $(\alpha\mu t)_{01}^{2+}$ deexcitation and decay induced by the $M_{01}H^+$ ionization also lead to the decay of the electronic ion. Deexcitation is energetically allowed because the ionization threshold of the $M_{01}H^+$ is expected to be very close to the ionization threshold of the $^4HeH^+$ ion, 40 eV [119, 120]. This process is analogous to the dissociative photoionization of the $^4HeH^+$ ion, which leads to $^4He^+ + p$, $^4He^{2+} + H$, or the dissociative state of $^4HeH^{2+}$. Based on this analogy and considering the energy conservation, $(\alpha\mu t)_{01}^{2+}$ deexcitation will produce $M_{01}H^+ \to M_{10}^+ + p + e$.

The decay of the $(\alpha\mu t)_{01}^{2+}$ molecule due to $M_{01}H^+$ ionization would lead to the decay of the electronic ion. The possible decay channels are (escaping electron is omitted) $(\alpha\mu)_{1s}^+ e + t + p$, $(\alpha\mu)_{1s}^+ + t + H$, $(\alpha\mu)_{1s}^+ + T + p$, $(\alpha\mu)_{1s}^+ + HT^+$, and $[(\alpha\mu)_{1s}^+, pe]^+ + t$, in which exotic molecular ion is produced. The calculation of the corresponding decay widths is a difficult task because three or four particles appear in the final channels. However, the widths can be calculated or estimated using appropriate approximations.

E1-transitions from continuum spectrum of the $t+\alpha$ system to the ground $I = (1/2)^-$ and the first excited $I = (3/2)^-$ state of the resulting lithium nucleus dominate in the total cross section for $(t\mu)_{1s} + \alpha$ fusion [49, 55]. Their relative contribution is about $3:2$. The corresponding photon energies are (2483.7 ± 4.5) keV and (2006.1 ± 4.1) keV. As it was mentioned in Introduction, the main difficulty in laboratory studies of nuclear reactions in scattering experiments at low-energies is due to Coulomb repulsion, which causes the fusion cross section $\sigma_f(E)$ to drop drastically below 100 keV [121]. Strong energy dependence corresponding to the low-energy penetrability through the Coulomb barrier can be factored out using the astrophysical S-factor, $\sigma_f(E) = S(E)E^{-1}\exp(-2\pi\eta)$, where E is the collision energy; $\eta = e^2/(\hbar\upsilon)$ is the Sommerfeld parameter; υ is the collision velocity. If no resonances occur, $S(E)$ is smooth function of energy and can be successfully extrapolated to zero energy. However, in the absencereaction occurring inside the of a credible theory, only experiment can decide whether such a procedure makes sense. The possibility of verifying the extrapolation may be given by experimental study of nuclear fusion occurring inside muonic

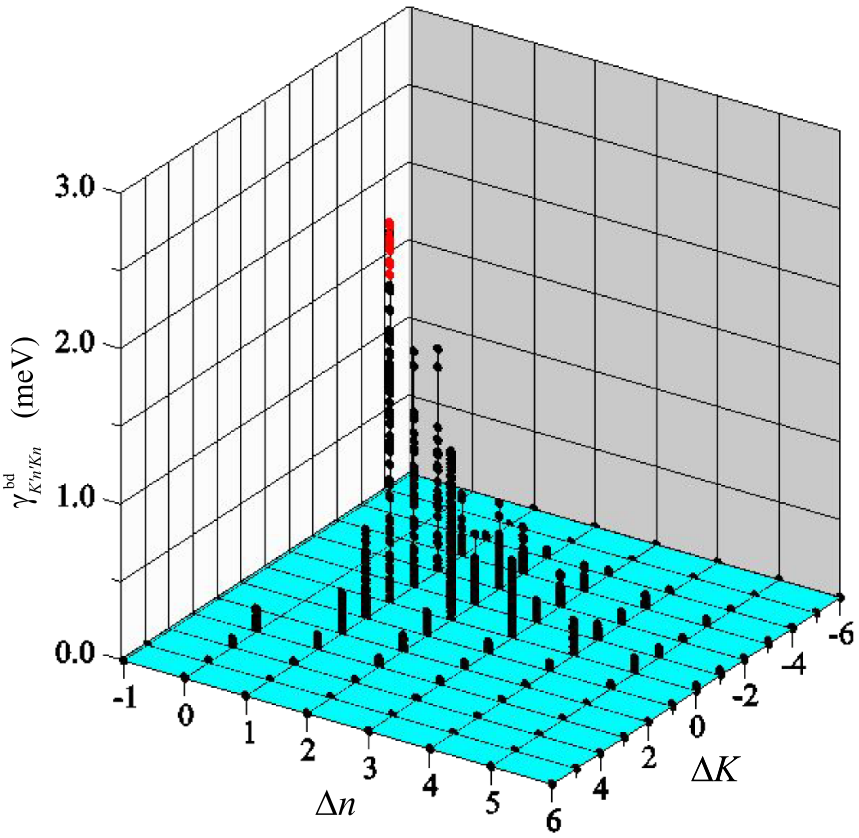

Figure 5. Approximated back-decay widths (21) presented on the $(\Delta K, \Delta n)$-plane. Red points correspond to the transitions in table 1.

molecule. Namely, the rate of nuclear fusion from the (j,ν) state of a muonic molecule corresponding to the relative orbital angular momentum L of nuclei has the form [121, 122] $\lambda_L^{j\nu} = K_L G_L^{j\nu}$, where $K_L = \pi^{-1} S_L(0)/(\tilde{\alpha}\,\mu_{\rm red})^{2L+1}$ is reaction constant expressed by the partial S-factor at zero collision energy $S_L(0)$; $\tilde{\alpha}$ is the fine structure constant; $\mu_{\rm red}$ is the reduced mass of the nuclei; $G_L^{j\nu}$ are certain molecular factors calculated at zero distance between the nuclei. Because $G_L^{j\nu}$ are very sensitive to the form of the muonic molecule wave function $\phi^{\rm mol}_{jm_j\nu}(\mathbf{R},\mathbf{r})$, the latter must be calculated with high precision. In the case of α and t bound in the $(\alpha\mu t)^{2+}_{01}$ muonic molecule, where $j=0$ and $\nu=1$, the fusion rate takes the form $\lambda_L^{01} = K_L G_L^{01}$. Since two molecular states: 1sσ (with $l=0$) and 2pσ (with $l=1$) contribute dominantly to the corresponding wave function at $R\to 0$ [101], the only values of L, where $L = |j-l|,\ldots,j+l$, which should be taken into account are 0 and 1. But, on the other hand, $K_1 << K_0$ [63], therefore only G_0^{01}, which is defined as $G_0^{01} = \int d^3r\,|\phi^{\rm mol}_{001}(R=0,\mathbf{r})|^2$ and corresponds to the 1sσ non-adiabatic component of the $(\alpha\mu t)^{2+}_{01}$ wave function, deserves attention. Once G_0^{01} has been calculated and λ_0^{01} has been measured, K_0 can be determined.

The study of the $(t\mu)_{1s}+\alpha$ reaction occurring inside the $(\alpha\mu t)^{2+}_{01}$ muonic molecule, which is resonantly formed in process (1) can be carried out using various experimental arrangements. For example, one can consider a thermalized tritium target that is irradiated with two beams, one composed of negative muons and the other of ^{4}HeH$^+$ ions. Muonic tritium atoms formed due to the capture of muons into highly excited atomic orbits ($n=14$) deexcite very quickly to the ground state (after approximately 10^{-10} s). In another example, a target consisting of ^{4}HeH$^+$ ions is irradiated with a beam of $t\mu$ atoms in the ground state, obtained by the atomic beam method [123–126].

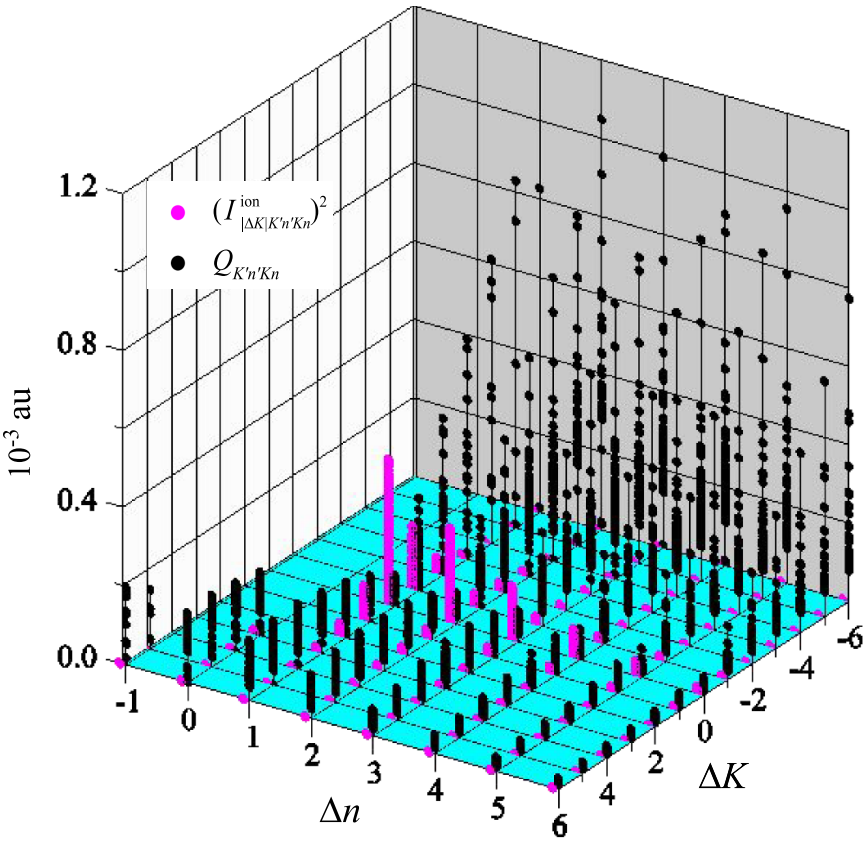

Figure 6. Coefficients $(I^{\text{ion}}_{\Delta KK'n'Kn})^2$ and $Q_{K'n'Kn}$ presented in the $(\Delta K, \Delta n)$-plane. The points representing $(I^{\text{ion}}_{|\Delta K|K'n'Kn})^2$ are slightly shifted along the Δn-axis to make the drawing more readable.

Table 2. $(K_{\text{top}}, n_{\text{top}})$ corresponding to $I^2{}_{\max}(\Delta K, \Delta n)$.

$\Delta n \rightarrow \Delta K \downarrow$	1	2	3	4
−3	(0,1)	(0,4)	(0,5)	(0,7)
−2	(1,2)	(2,5)	(2,7)	(2,8)
−1	(6,4)	(9,7)	(0,4)	(0,6)
0	(0,2)	(0,5)	(0,6)	(0,7)
1	(1,5)	(5,3)	(4,4)	(3,6)
2	(2,3)	(2,5)	(2,7)	(2,8)
3	(3,2)	(3,4)	(3,5)	(3,7)

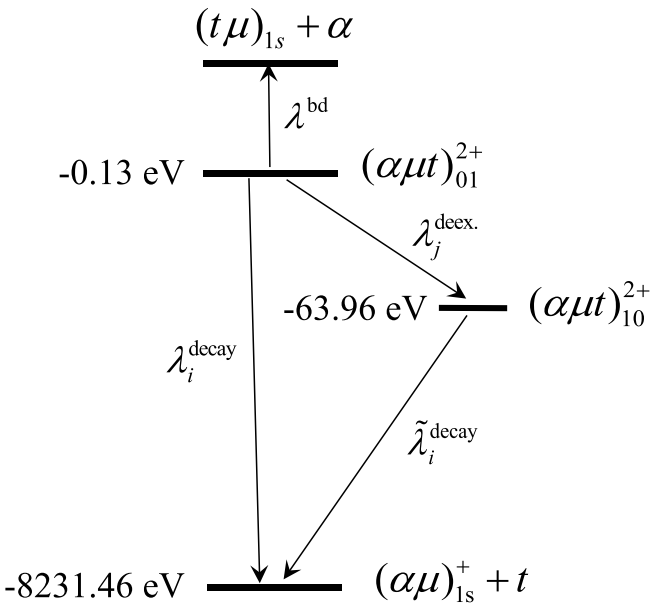

Figure 7. Energy levels diagram (not to scale) and transitions in the muonic molecule $(\alpha\mu t)^{2+}_{01}$ resonantly formed in $M_{01}H^{+}$ ion (fusion $t(\alpha,\gamma)^{7}$Li is not shown). Subscripts of reaction rates, $i=\gamma,e,$pr. and $j=\gamma,e$ indicate the transitions induced by photon emission (γ), ionization of the $M_{01}H^{+}$ ion (e), and predissociation (pr.). Energies are calculated relative to the $(t\mu)_{1s}$ threshold, $E_{(t\mu)_{1s}}=-2711.17\,\mathrm{eV}$.

Data availability statement

All data that support the findings of this study are included within the article (and any supplementary files).

Acknowledgment

The author is very grateful to N Popov for the fruitful discussions. This work was partially financed (supported) by the subsidy of the Ministry of Science and Higher Education (Poland).

ORCID iD

Wilhelm Czapliński https://orcid.org/0000-0001-9670-478X

References

[1] Workman R L *et al* 2022 Particle data group *Prog. Theor. Exp. Phys.* **2022** 083C01 (2022) (available at: https://pdg.lbl.gov/2022)
[2] Alvarez L W *et al* 1957 *Phys. Rev.* **105** 1127
[3] Breunlich W H, Kammel P, Cohen S and Leon M 1989 *Annu. Rev. Nucl. Part. Sci.* **39** 311
[4] Nagamine K and Kamimura M 1998 *Adv. Nucl. Phys.* **24** 151
[5] Popov N 2019 *Muon Physics* (Cambridge Scholar Publishing)
[6] Nagamine K 2003 *Introductory Muon Science* (Cambridge University Press)
[7] Strakovsky I I, Baturin V N, Brewer J H, Denisov D, Karpeshin F, Popov N and Shiltsev V D 2020 *Modern Muon Physics—Selected Issues* (NOVA)
[8] Gorringe T P and Hertzog D W 2015 *Prog. Part. Nucl. Phys.* **84** 73
[9] Safronova M S, Budker D, DeMille D, Jackson Kimball D F, Derevianko A and Clark C W 2018 *Rev. Mod. Phys.* **90** 025008
[10] Andreev V A *et al* 2013 *Phys. Rev. Lett.* **110** 012504
[11] Adelberger E G *et al* 1998 *Rev. Mod. Phys.* **70** 1265
[12] Adelberger E G *et al* 2011 *Rev. Mod. Phys.* **83** 195
[13] Alvarez-Ruso L *et al* 2022 Neutrino scattering measurements on hydrogen and deuterium: a snowmass white paper (arXiv:2203.11298)
[14] Karr J P and Marchand D 2019 *Nature* **575** 61
[15] Bezginov N, Valdez T, Horbatsch M, Marsman A, Vutha A C and Hessels E A 2019 *Science* **365** 1007
[16] Xiong W *et al* 2019 *Nature* **575** 147
[17] Pohl R *et al* 2010 *Nature* **466** 213
[18] Kravtsov A V, Popov N P, Solyakin G E, Aristov Yu A, Faifman M P and Truskova N F 1981 *Phys. Lett.* **A 83** 379
[19] Czapliński W, Gronowki J, Kamiński W and Popov N 2010 *Phys. Lett.* A **375** 155
[20] Czapliński W, Kravtsov A, Mikhailov A and Popov N 1998 *Phys. Lett.* A **219** 86
[21] Czapliński W, Kravtsov A, Mikhailov A and Popov N 1998 *Eur. Phys. J.* D **3** 223
[22] Vinitskiĭ S I, Melezhik V S, Ponomarev L I, Puzynin I V, Puzynina T P, Somov L N and Truskova N F 1980 *Sov. Phys. JETP* **52** 353
[23] Gocheva A D, Gusev V V, Melezhik V S, Ponomarev L I, Puzynin I V, Puzynina T P, Somov L N and Vinitsky S I 1985 *Phys. Lett.* B **153** 349
[24] Bandrauk A D and Paramonov G K 2014 *Int. J. Mod. Phys.* **23** 1430014
[25] Chelkowski S, Bandrauk A D and Corkum P B 2004 *Phys. Rev. Lett.* **93** 083602
[26] Clayton D D 1983 *Principles of Stellar Evolution and Nucleosynthesis* (University of Chicago Press)
[27] Rolfs C, Trautvetter H P and Rodney W S 1987 *Rep. Prog. Phys.* **50** 233
[28] Olive K A, Steigman G and Walker T P 2000 *Phys. Rep.* **333–334** 389
[29] Fields B D and Olive K A 2006 *Nucl. Phys.* A **777** 208

[30] Iocco F, Mangano G, Miele G, Pisanti O and Serpico P D 2009 *Phys. Rep.* **472** 1
[31] Cyburt R H, Fields B D, Olive K A and Yeh TH 2016 *Rev. Mod. Phys.* **88** 015004
[32] Mathews G J, Kusakabe M and Kajino T 2017 *Int. J. Mod. Phys.* E **26** 1741001
[33] Fields B D, Olive K A, Yeh TH and Young C 2020 *J. Cosmol. Astropart. Phys.* **2020** 010
[34] Fields B D, Olive K A, Yeh TH and Young C 2020 *J. Cosmol. Astropart. Phys.* **2020** E02
[35] Iliadis C and Coc A 2020 *Astrophys. J.* **901** 127
[36] Bertulani C A, Hall F W and Santoyo B I 2023 *EPJ Web Conf.* **275** 01003
[37] Fields B D 2011 *Annu. Rev. Nucl. Part. Sci.* **61** 47
[38] Coc A, Goriely S, Xu Y, Saimpert M and Vangioni E 2012 *Astrophys. J.* **744** 158
[39] Sbordone L *et al* 2010 *Astron. Astrophys.* **522** A26
[40] Matteucci F, Molero M, Aguado D S and Romano D 2021 *Mon. Not. R. Astron. Soc.* **505** 200
[41] Flambaum V V 2008 *Eur. Phys. J.: Spec. Top.* **163** 159
[42] Berengut J C, Flambaum V V and Dmitriev V F 2010 *Phys. Lett.* B **683** 114
[43] Mori K and Kusakabe M 2019 *Phys. Rev.* D **99** 083013
[44] Clara M T and Martins C J A P 2020 *Astron. Astrophys.* **633** L11
[45] Koren S 2023 *Phys. Rev. Lett.* **131** 091003
[46] Brune C R, Kavanagh R W and Rolfs C 1994 *Phys. Rev.* C **50** 2205
[47] Descouvemont P, Adahchour A, Angulo C, Coc A and Vangioni-Flam E 2004 *At. Data Nucl. Data Tables* **88** 203
[48] Xu Y, Takahashi K, Goriely S, Arnould M, Ohta M and Utsunomiya H 2013 *Nucl. Phys.* A **918** 61
[49] Solovyev A S, Igashov S Y and Tchuvil'sky Y M 2015 *EPJ Web Conf.* **86** 00054
[50] Turakulov S A and Tursunov E M 2019 *Int. J. Mod. Phys. Conf. Ser.* **49** 1960014
[51] Tursunov E M, Turakulov S A and Kadyrov A S 2018 *Phys. Rev.* C **97** 035802 (https://www.worldscientific.com/doi/abs/10.1142/S2010194519600140)
[52] Sadeghi H 2013 *Chin. Phys. Lett.* **30** 102501
[53] Solovyev A S, Igashov S Y and Tchuvil'sky Y M 2014 *J. Phys.: Conf. Ser.* **569** 012020
[54] Neff T 2011 *Phys. Rev. Lett.* **106** 042502
[55] Bystritsky V M, Dudkin G N, Emets E G, Filipowicz M, Krylov A R, Nechaev B A, Nurkin A, Padalko V N, Philippov A V and Sadovsky A B 2017 *Phys. Part. Nucl. Lett.* **14** 560
[56] Dohet-Eraly J, Navrátil P, Quaglioni S, Horiuchi W, Hupin G and Raimondi F 2016 *Phys. Lett.* B **757** 430
[57] Hu C Y and Bhatia A K 1990 *Phys. Rev.* A **42** 5769
[58] Kino Y and Kamimura M 1993 *Hyperfine Interact.* **82** 195
[59] Belyaev V B, Korobov V I and Rakityansky S A 1994 *Few-Body Syst.* **17** 243
[60] Decker M, Sandhas W and Belyaev V B 1996 *Phys. Rev.* A **53** 726
[61] Kartavtsev O I, Kochin V I and Kolganova E A 1999 *Hyperfine Interact.* **118** 235
[62] Wallenius J and Froelich P 1999 *Hyperfine Interact.* **118** 223
[63] Bogdanova L N, Gerstein S S and Ponomarev L I 1998 *JETP Lett.* **67** 99
[64] Bogdanova L N, Korobov V I and Ponomarev L I 1999 *Hyperfine Interact.* **118** 183
[65] Maev E M *et al* 1999 *Hyperfine Interact.* **118** 171
[66] Knowles P E *et al* 2001 *Hyperfine Interact.* **138** 289
[67] Bystritsky V M, Filipowicz M, Gerasimov V V, Knowles P E, Mulhauser F, Popov N P, Volnykh V P and Woźniak J 2006 *Eur. Phys. J.* D **38** 455
[68] Gronowski J, Czapliński W and Popov N 2004 *Acta Phys. Pol.* A **106** 795
[69] Czapliński W and Rybski M 2016 *Phys. Lett.* A **380** 869
[70] Faifman M P, Menshikov L I and Strizh T A 1989 *Muon Catal. Fusion* **4** 1
[71] Grandinetti F 2004 *Int. J. Mass Spectrom.* **237** 243
[72] Hogness T R and Lunn E G 1925 *Phys. Rev.* **26** 44
[73] Ketterle W, Dodhy A and Walther H 1988 *J. Chem. Phys.* **89** 3442
[74] Strasser D, Bhushan K G, Pedersen H B, Wester R, Heber O, Lafosse A, Rappaport M L, Altstein N and Zajfman D 2000 *Phys. Rev.* A **61** 060705
[75] Zajfman D, Heber O, Vejby-Christensen L, Ben-Itzhak I, Rappaport M, Fishman R and Dahan M 1997 *Phys. Rev.* A **55** R1577
[76] Dahan M, Fishman R, Heber O, Rappaport M, Altstein N, Zajfman D and Vander Zande W J 1998 *Rev. Sci. Instrum.* **69** 76
[77] Wolf B (ed) 1995 *Handbook of Ion Sources* (CRC Press)
[78] Pedersen H B *et al* 2007 *Phys. Rev. Lett.* **98** 223202
[79] Müller J C, Dörner R, King F, Schmidt L, Ph H, Schöffler M S and Stiebing K E 2017 *J. Phys.: Conf. Ser.* **875** 092003
[80] Wustelt P, Oppermann F, Yue L, Möller M, Stöhlker T, Lein M, Gräfe S, Paulus G G and Sayler A M 2018 *Phys. Rev. Lett.* **121** 073203
[81] Liebl H and Harrison W W 1976 *Int. J. Mass Spectrom. Ion. Phys.* **22** 237
[82] Stancil P C, Lepp S and Dalgarno A 1998 *Astrophys. J.* **509** 1
[83] Galli D and Palla F 1998 *Astron. Astrophys.* **335** 403 (https://ui.adsabs.harvard.edu/abs/1998A%26A...335..403G/abstract)
[84] Lepp S, Stancil P C and Dalgarno A 2002 *J. Phys. B: At. Mol. Opt. Phys.* **35** R57
[85] Dalgarno A 2005 *J. Phys.: Conf. Ser.* **4** 10
[86] Galli D and Palla F 2013 *Annu. Rev. Astron. Astrophys.* **51** 163
[87] Roberge W and Dalgarno A 1982 *Astrophys. J.* **255** 489
[88] Kraemer W P, Špirko V and Juřek M 1995 *Chem. Phys. Lett.* **236** 177
[89] Wildt R 1949 *Astron. J.* **54** 139
[90] Dabrowski I and Herzberg G 1977 *Trans. New York Acad. Sci.* **38** 14
[91] Black J H 1978 *Astrophys. J.* **222** 125
[92] Moorhead J M, Lowe R P, Wehlau W H, Maillard J P and Bernath P F 1988 *Astrophys. J.* **26** 899
[93] Zinchenko I, Dubrovich V and Henkel C 2011 *Mon. Not. R. Astron. Soc.* **415** L78
[94] Zicler E, Parisel O, Pauzat F, Ellinger Y, Bacchus-Montabonel MC and Maillard JP 2017 *Astron. Astrophys.* **607** A61
[95] Güsten R, Wiesemeyer H, Neufeld D, Menten K M, Graf U U, Jacobs K, Klein B, Ricken O, Risacher C and Stutzki J 2019 *Nature* **568** 357
[96] Neufeld D A, Goto M and Geballe T R 2020 *Astrophys. J.* **894** 37
[97] Lane A M 1987 *J. Phys. B: At. Mol. Opt. Phys.* **20** 2911
[98] Faifman M P and Ponomarev L I 1991 *Phys. Lett.* B **265** 201
[99] Wallenius J and Froelich P 1996 *Phys. Rev.* A **54** 1171
[100] Gheisari R 2007 *Mol. Phys.* **105** 2927
[101] Ponomarev L I and Vinitsky S I 1979 *J. Phys. B: At. Mol. Opt. Phys.* **12** 567
[102] Landau L D and Lifshitz E M 1977 *Quantum Mechanics: Nonrelativistic Theory* (Pergamon)
[103] Power J D 1973 *Phil. Trans. R. Soc.* **274** 663
[104] Kamimura M 1988 *Phys. Rev.* A **38** 621
[105] Bransden B H and Joachain C J 2003 *Physics of Atoms and Molecules* (Prentice Hall)
[106] Pachucki K 2012 *Phys. Rev.* A **85** 042511
[107] Cohen J S and Martin R L 1984 *Phys. Rev. Lett.* **53** 738

[108] Edmonds A R 1985 *Angular Momentum in Quantum Mechanics* (Princeton Landmarks in Physics)
[109] Abramowitz M and Stegun I A 1970 *Handbook of Mathematical Functions with Formulas, Graphs, and Mathematical Tables* (Dover)
[110] Varshalovich D A, Moskalev A N and Khersonskii V K 2008 *Quantum Theory of AngularMomentum* (World Scientific)
[111] Bohm A 1993 *Quantum Mechanic, Foundations and Applications* 3rd edn (Springer)
[112] Carrington A, Kennedy R A, Softley T P, Fournier P G and Richard E G 1983 *Chem. Phys.* **81** 251
[113] Liu Z and Davies P B 1997 *Phys. Rev. Lett.* **79** 2779
[114] Zygelman B, Stancil P C and Dalgarno A 1998 *Astrophys. J.* **508** 151
[115] Belyaev V B, Kartavtsev O I, Kochin V I and Kolganova E A 1997 *Z. Phys.* D **41** 239
[116] Czapliński W, Kravtsov A, Mikhailov A and Popov N 1997 *Phys. Lett.* A **233** 405
[117] Bethe H A and Salpeter E E 2008 *Quantum Mechanics of One- and Two-Electron Atoms* (Dover)
[118] Kravtsov A V, Mikhailov A I and Savichev V I 1994 *Z. Phys.* D **29** 49
[119] Saenz A 2003 *Phys. Rev.* A **67** 033409
[120] Fernández J and Martín F 2007 *J. Phys. B At. Mol. Opt. Phys.* **40** 2471
[121] Bogdanova L N 2013 *Phys. At. Nucl.* **76** 376
[122] Bogdanova L N 1988 *Muon Catal. Fusion* **3** 359
[123] Fujiwara M C *et al* 2000 *Phys. Rev. Lett.* **85** 1642
[124] Fujiwara M C *et al* 2000 Using thin film targets for muonic atoms and muon catalyzed fusion studies *High Intensity Muon Sources* edY Kuno and T Yokoi (World Scientific) p 291
[125] Fujiwara M C *et al* 2001 Time-of-flight spectroscopy of muonic hydrogen atoms and molecules *The Hydrogen Atom* (*Lecture Notes in Physics* vol 570) (Springer) p 435
[126] Schmidt S *et al* 2018 *J. Phys.: Conf. Ser.* **1138** 012010